Investigation of Cutting Quality of Remote DOE Laser Cutting in 0.5 mm Stainless Steel

Villumsen, Sigurd; Kristiansen, Morten

Published in:
Physics Procedia

DOI (link to publication from Publisher):
10.1016/j.phpro.2017.08.007

Publication date:
2017

Document Version
Publisher's PDF, also known as Version of record

Available online at www.sciencedirect.com

ScienceDirect

Physics Procedia 89 (2017) 164 – 171

Physics Procedia

Nordic Laser Materials Processing Conference, NOLAMP_16, 22-24 August 2017, Aalborg University, Denmark

Investigation of cutting quality of remote DOE laser cutting in 0.5mm stainless steel

Sigurd Lazic Villumsen[a]* & Morten Kristiansen[a]

[a]*Aalborg University, Department of Mechanical and Manufacturing Engineering, Fibigerstræde 16, Aalborg 9220, Denmark.*

Abstract

It has previously been shown that the stability of the remote fusion cutting (RFC) process can be increased by modifying the intensity profile of the laser by means of a diffractive optical element (DOE). This paper investigates the quality of remote DOE cutting (RDC) conducted with a 3kW single mode fiber laser in 0.5 mm stainless steel. An automatic measurement system is used to investigate how the travel speed, focus offset and angle of incidence effect the kerf width and kerf variance. The study shows that the RDC process has a very low kerf width variance, and that the kerf width decreases with cutting speed. Furthermore, selected etched samples show a significant increase in the perpendicularity of the cuts when compared to RFC. Also, on average, the depth of the layer of molten material for RFC is 83% deeper than for RDC.

Peer-review under responsibility of the scientific committee of the Nordic Laser Materials Processing Conference 2017

Keywords: Remote laser cutting, Remote fusion cutting, Diffractive optical element, Laser cutting, Beam shaping

1. Introduction

Two methods are often mentioned when considering remote laser cutting (RLC): remote fusion cutting (RFC) and remote ablation cutting (RAC). In traditional laser cutting, molten material is ejected by the application of gas through a nozzle. As the remote position of the cutting head in RLC makes this approach infeasible, these processes will need to rely on other methods of ejecting molten material from the cutting kerf (Zaeh et al (2010) and Lu et al (2013)). As regards remote fusion cutting (RFC), the melt ejection is achieved by laser-induced pressure generated from the

* Corresponding author. Tel.: +45 30130852
E-mail address: sv@make.aau.dk

Peer-review under responsibility of the scientific committee of the Nordic Laser Materials Processing Conference 2017
doi:10.1016/j.phpro.2017.08.007

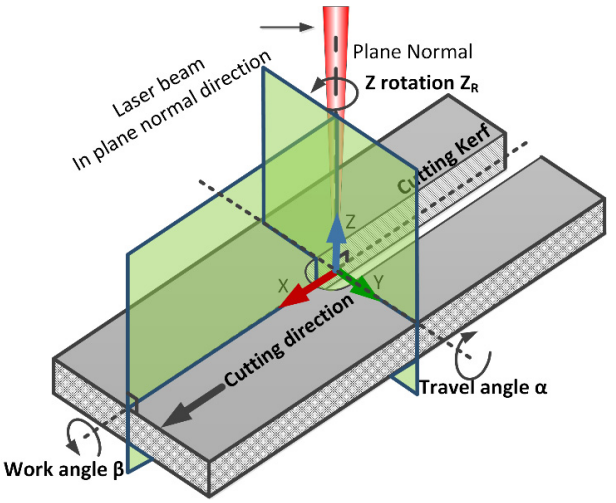

Figure 1. The definition of work and travel angles used. . Here it is seen that both angles are defined as the angular deviation from the normal vector of the work piece, thus a perpendicular beam will have a travel angle and a work angle equal to 0°.

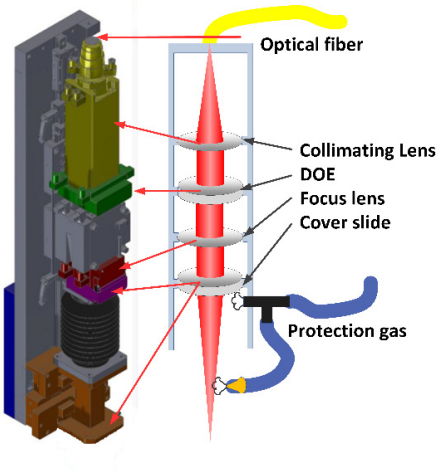

Figure 2. The cutting head used in this paper. The colors of the cutting head indicate the following modules: Yellow – Collimating module, Green – DOE module, Red – Focus module, Brown and purple – Cover slides.

evaporation of material inside the cutting kerf (Matti et al (2013)). The melt is expelled through the bottom of the kerf and not upwards as with RAC (Schäfer 2010). This melt flow out of the cutting kerf can be seen as similar to the horizontal melt flow around the keyhole in keyhole laser welding (Preissig et al (1994)). In RFC, a further downwards flow is created due to the vapor pressure in the processing area (Schober et al 2012). However, the melt ejection of RFC has been described as unstable, and thus repeatable experiments can be difficult to obtain (Pihlava et al (2013) & Villumsen et al (2015)). With regard to the stability of RFC related to the incident angle of the laser beam, Villumsen et al (2015) have shown that for cuts in 0.5mm SST with a 3kW single mode fiber laser, stable and repeatable cuts have been obtained within a boundary of $\pm$ 6°.

To stabilize and control the melt flow inside the cutting kerf, additional guiding laser irradiation inside the cutting kerf can be introduced (Olsen et al 2009). Essentially, this means that by choosing an appropriate intensity distribution, a more efficient melt ejection can be obtained. The melt guiding laser irradiation can be applied as a set of guiding beams (Olsen et al 2009) or as an altered intensity profile. To increase the melt ejection of RFC, it has been shown in Villumsen et al (2016) that a diffractive optical element can be inserted in the collimated beam path to change the intensity distribution of the cutting beam. The resulting remote DOE cutting (RDC) process increased the stability with regard to incident angle from 6° to much as 32° on the same 3kW setup.

This paper will investigate and expand on the results presented in Villumsen et al (2016). Whereas the former paper only discussed cut stability, this paper will explore the quality with regard to the following parameters:

- Kerf width
- Variations in kerf width
- Burr formations
- Melt zone
- Perpendicularity

The paper will be organized in the following way: In section 2, the methodology of the conducted experiments will be described along with equipment and definitions. In section 3, the obtained results will be presented and compared to the results generated in Villumsen et al (2016). Finally, section 4 will present a discussion and a conclusion.

2. Definitions and Methodology

The results presented in this paper will be based on the two sets of experiments presented in Villumsen et al (2016). These showed the effects of focus offset, cutting speed, travel angle, and work angle on the stability of the remote DOE cutting process. However, to describe the quality of the RDC process it is necessary to conduct further analysis on the obtained samples. The parameters used in the two sets of experiments can be seen from table 1.

In the first set of experiments the effect of beam diameter and travel speed on the quality of the RDC process was investigated. Here the incident angle was kept constant at 0°, while the beam diameter was adjusted by moving the focus offset of the cutting head 1mm at a time. The **incident angle** was decomposed into two angles, a **travel angle α** and **a work angle β** as seen in Figure 1. From this figure it appears that both angles are defined as the angular deviation from the normal vector of the work piece, thus a perpendicular beam will have a travel angle and a work angle equal to 0°. The focus offset was defined as the distance from beam waist to the surface of the sheet metal.

In the second set of experiments, the effect of the work and travel angles on remote DOE cutting quality was investigated. By defining a robot tool calibration from the robot TCP to the beam waist it was possible to adjust, the work and travel angles by means of the robot teach pendant without changing the focus.

Table 1: A summary of the two sets of experiments described in Villumsen et al (2016). Items marked [a] were found from the first set of experiments. The marking [b] indicates that experiments were discontinued when no stable cuts were obtained.

	Travel speed[a]	**Focus offset[a]**	**Work angle**	**Travel Angle**	**Repetitions**	**Number of cuts**
Experiment 1	800-1800 mm/min steps of 200 mm/min	0 - +10 mm in steps of 1mm	0°	0°	3	198
	Travel speed[a]	**Focus offset[a]**	**Work angle[b]**	**Travel Angle[b]**	**Repetitions**	**Number of cuts**
Experiment 2	1200 mm/min	+5 mm	0-34° steps of 2°	0-16° steps of 2°	6	1026

2.1. Equipment

Both two sets of experiments described in the previous section were conducted with the experimental setup seen on Figure 2. From this figure it appears that the DOE was situated in a module (marked by red) which was inserted in the collimated beam path. Compressed air was applied through both the cutting head and a cross jet to prevent dust and ejected molten material from contaminating the optics. It should be noted that compressed air was only applied for protection purposes and not as a cutting gas. In all experiments, the movements were conducted with an XY table situated underneath the cutting head. A list of the equipment used and the invariant cutting parameters can be found in Table 2.

Table 2 Equipment and cutting parameters

Equipment	**Type and manufacturer**	**Parameter**	**Value**
Industrial robot	KUKA Quantec kr120 R2500	Power	3kW
Laser	3kW IPG YLS-3000 (Single mode)	Material	SST EN Type:X2CrNi19-11 No. 1.4307
Cutting head	HighYag 470mm focal length	Thickness	0.5mm
XY positioning system	Q-sys	Cutting gas	None (Air cross jet)
		Laser mode	Pulsed (21% duty cycle)

2.2. Beam pattern

To generate the beam pattern required for the RDC process, a diffractive optical element (DOE) was inserted into the beam path after the collimating lens. Table 3 lists the production specifications of the DOE.

Table 3: Details describing the used DOE

Manufacturer	Material	Production process	Diameter
II-VI	Zinc sulfide (ZnS)	Diamond turning	50mm

By inserting the DOE into the collimated beam path, the Gaussian intensity distribution of the single mode fiber laser was transformed into the profile seen in Figure 2.

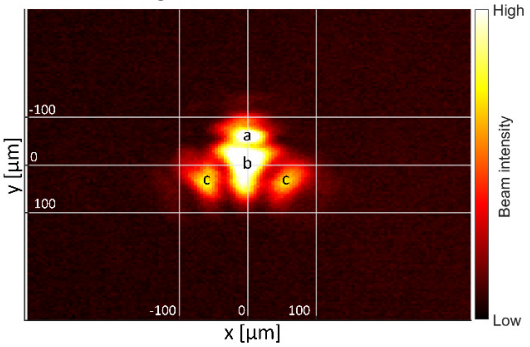

Figure 3: The intensity distribution of the resulting beam after the DOE. Notice that the the image is captured in the cutting region, +7 mm away from the beam waist. The beam is composed of three components the melt beam a, the lid beam b, and the trailing beams c.

The shape of the intensity distribution shown in Figure 3 originates from an iterative design process. The shape is composed of three main components to which the material is exposed during cutting. These components have been named the melt beam a, the lid beam b, and the trailing beams c. During cutting, the material is first exposed to the melt beam. Due to the intensity of the melt beam, a keyhole is formed which forces molten material towards the sides and back of the cut. The intensity of the lid beam evaporates further material, and thus a vapor pressure is induced on top of the molten material in the kerf, forcing the molten material downwards. The trailing beams are used for further guiding the melt and edge trimming. For more information about the chosen beam pattern see Villumsen et al (2016).

2.3. Data analysis

To ensure that all cut samples were analyzed, the automated stability evaluation system described in Villumsen et al (2015) was used. However, to ensure that parameters related to the cutting quality could be obtained, modification was necessary. The first step in the automatic evaluation was to capture and stitch images of the entire cutting kerf on all samples. This was carried out using a programmable Carl Zeiss Axio imager microscope with an x2.5 objective and an image stitching algorithm implemented in Matlab. The resulting image can be seen from Figure 4. Subsequently, by using dynamic thresholding and contrast enhancement, a BW image was obtained in which all white pixels correspond to an unblocked cutting kerf. By summing up all white pixels in the Y direction, a measure of the kerf width can be obtained. By combining this with a scaling factor for the x2.5 objective, a distance in µm can be obtained. It should be noted that the minimum stability length l_{min} mentioned in Villumsen et al (2015) was removed to include all open cut segments in the measurement of the kerf width.

As the proposed image processing analysis cannot describe other qualitative parameters than the width and variation of the kerf width, it was furthermore decided to analyze several samples by cutting them, polishing them and performing a surface etching process. These were then analyzed under a microscope to obtain a measure for the melt zone, the perpendicularity of the cut and a more precise measure of the kerf width. The perpendicularity was measured as defined by the *u* value in ISO 9013. Two measures will be derived for *u:* $u_{a=0.1,}$ which disregards the top and bottom 0.1 mm of the plate as indicated by the standard, and $u_{a=0,}$ which takes the entire thickness of the sheet into account.

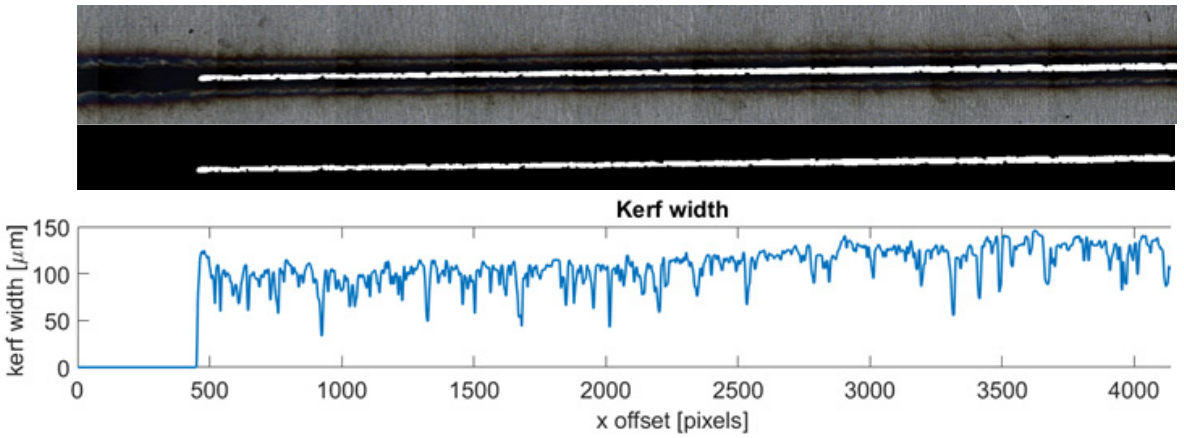

Figure 4. The basic principle of the automatic kerf width evaluation algorithm. A stitched image is obtained of the cut. This image is transformed to a thresholded image which shows cut/not cut areas. By summing up the white pixels of the image, a measure for the kerf width can be obtained.

3. Results

In the following section, the obtained quality parameters will be described and discussed. In section 2 it was defined that the quality of the remote doe cuts should be analyzed with respect to the Kerf width, Variations in kerf width, Burr formations, width of Melt zone, and cut perpendicularity.

3.1. Top kerf width and top kerf variance

By using the image processing system described in section 2.5, all 1200 cuts were analyzed, and width data was collected over the entire cut. The average cut width for all repetitions for the first and second experiments can be seen from Figures 3 and 4, respectively. When considering experiment 1, it can be seen that the average kerf width lies between 100 and 200 µm for almost all data points. It is also seen that the width generally decreases with increased velocity. When considering the standard deviation of the cutting kerf width, it is seen that the width of the kerf does not vary much, except for low focus offsets. Notice that as the process in this region is not very stable the high variance originates from openings and closing of the cutting kerf. The results from experiment 2 can be seen from Figures 5-d to 5-f, which show that the average kerf width lies between 100 and 200 µm as for Experiment 1. A general trend can be seen towards narrower kerfs when increasing travel angle, but this is mainly due to the rapidly deteriorating stability of the process, as seen from Figure 5-d. As regards to the kerf variance, it appears that stable areas generally have a low variance as compared to unstable regions.

3.2. Melt zone, perpendicularity & side kerf width

To determine the size of the melt zone and the perpendicularity, 20 samples were cut, polished and etched. Figure 6 shows these along with 4 reference cuts obtained by RFC without DOE. The 20 samples were chosen to determine variations with regard to velocity, varying focus, travel angle, and work angle. Table 4 sums up the investigated parameters. As regards the perpendicularity of the cuts measured as $u_{a=0,}$ the RFC cuts obtained an average measure of 192 µm. The perpendicularity of the RDC samples was found to be 146 µm for the velocity samples (f-j). The average of all samples was found to be 163 µm.

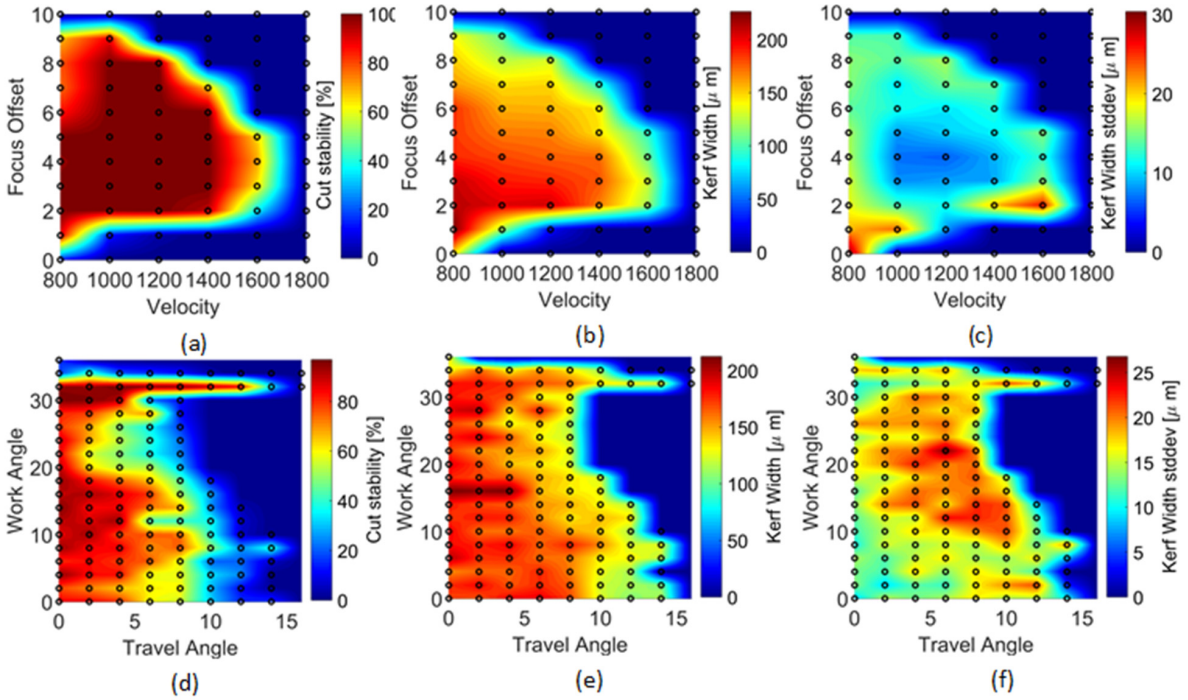

Figure 5. Plots of the obtained cutting data. (a) shows the cutting stability when varying focus offset and velocity. (b) is the cutting kerf width when varying focus offset and velocity. (c) depicts the standard deviation of the kerf width from (b) when varying focus offset and velocity. (d) shows the cutting stability when the travel and work angles are varied. (e) is the width of the cutting kerf when the travel and work angles are varied. And finally, (f) is the standard deviation of the width of the cutting kerf when the travel and work angles are varied.

Table 4. The measured quality parameters for 20 RDC samples and 4 RFC samples seen in figure 6. *u* are the perpendicularity measures as defined by ISO 9013 (ISO (2002)). W is the cutting kerf width, and d is the maximum thickness of the molten material on the sides of the kerf.

	Focus					Velocity					Work Angle					Travel Angle					RFC			
	a	**b**	**c**	**d**	**e**	**f**	**g**	**h**	**i**	**j**	**k**	**l**	**m**	**n**	**o**	**p**	**q**	**r**	**s**	**t**	**u**	**v**	**w**	**x**
$u_{a=0.1}$	79.0	64.3	76.9	89.5	73.4	~	~	86.01	79.0	63.6	86.0	61.6	85.3	85.3	93.7	86.01	74.12	78.3	80.4	67.8	69.76	52.3	58.13	81.3
$u_{a=0}$ [µm]	146.9	137.0	131.5	162.2	178.3	~	~	162.9	156.6	142.7	162.9	178.3	162.9	185.3	200.6	162.9	179	167.8	137.7	143.3	186.0	162.8	250	168.6
w [µm]	213.9	241.4	224.9	134.4	32.9	~	~	128.26	159.12	131.69	128.2	213.9	219.4	227.7	174.9	128.26	253.09	233.2	201.65	263.37	363	279	181	179
d	119.6	118.9	112.6	102.1	114.7	~	~	117.5	109.1	113.3	117.5	118.9	109.1	109.8	139.9	117.5	114.6	183.9	130.1	135.7	168.6	244.2	168.6	273.3

This increase in perpendicularity can also be seen from the shape of the kerf as the sample is generally less molten than the RFC samples. The same difference is not seen for $u_{a=0.1}$ as the large area of molten material on the top and bottom of the RFC cutting kerfs was not taken into account. In fact, RFC showed a slightly better perpendicularity (5 µm for velocity samples). Furthermore, it is seen that the perpendicularity decreases with larger work angles.

This tendency is reversed for the travel angle. When considering the melt zone, it can be seen from the table that

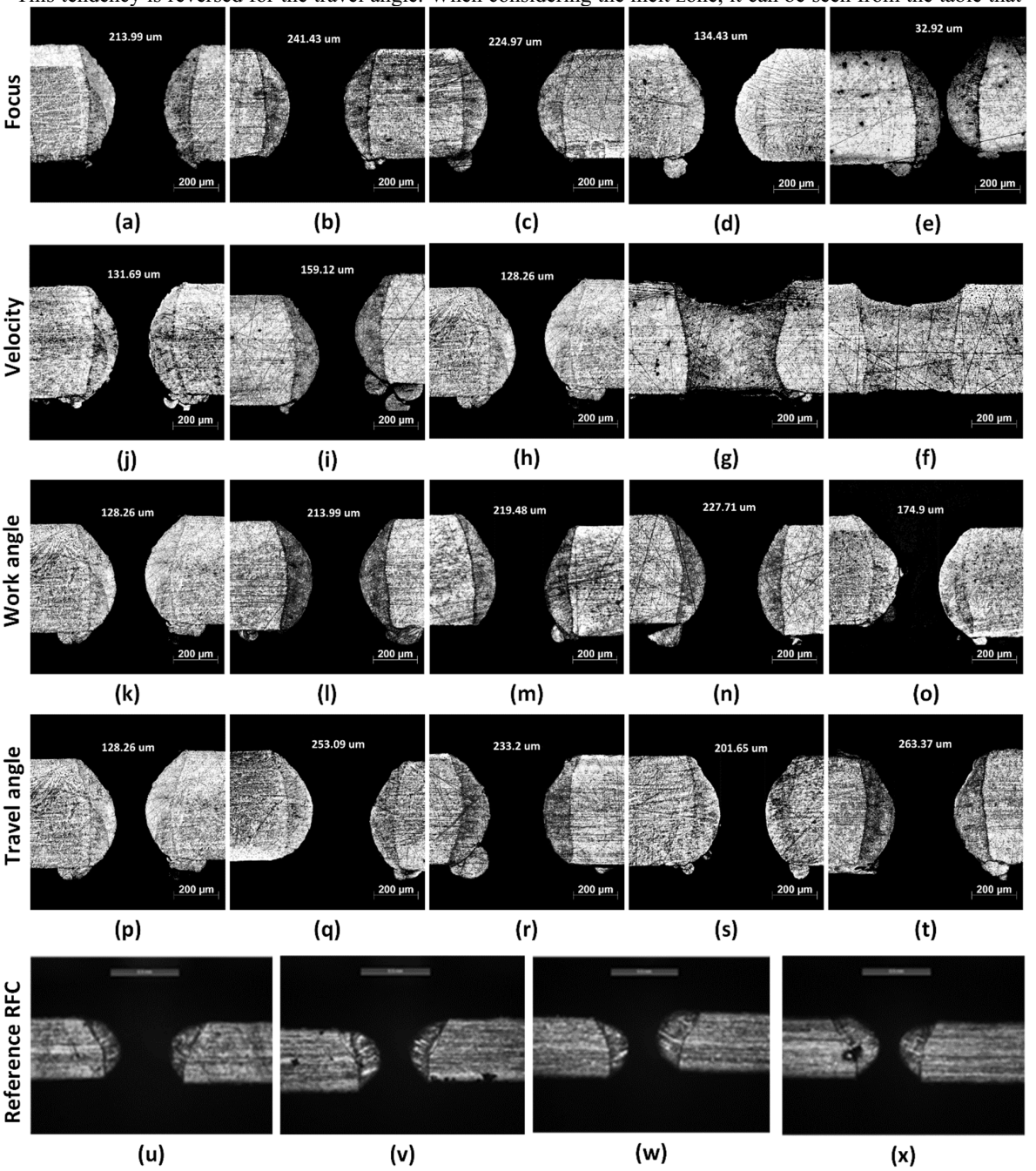

Figure 6: Microscopic images of 20 RDC samples and 4 RFC samples. The samples are divided into four categories depending on what properties have been varied. The following parameters have been used to obtain the above samples. vel=1200mm/min. focus =+5mm, Travel angle =0, Work angle =0. Other parameters can be found in table 4. Focus: (a): f=+2 mm. (b): f=+3 mm. (c):f=+4 mm. (d): f=+6 mm. (e): f=+7mm. Velocity: (f):vel=800mm/min. (g):vel=1000mm/min. (h):vel=1200mm/min. (i):vel=1400mm/min. (j):vel=1600mm/min. Work Angle: (k):WA=0°.(l):WA=2°.(m):WA=4°.(n):WA=6°.(o):WA=8°. Travel Angle: (p):TA=0°.(q):TA=2°.(r):TA=4°.(s):TA=6°.(t):TA=8°. RFC: focus position +15 mm. duty cycle =100% (u): vel =6500mm/min. (v): vel =7500mm/min. (w): vel =8500mm/min. (x): vel =9500mm/min

the RFC cuts have a much larger layer of molten material on the sides of the kerf. On average, the RFC melt zone is 213 µm deep. For the velocity samples of RDC an average of 116 µm was observed, and for all samples the average was 125 µm. In other words, the melt zone for RFC is approximately 83% deeper than that applying to RDC when considering the velocity samples (70% if all samples were considered). Furthermore, it was seen that the melt zone for the performed cuts remained quite constant over the cutting parameters. However, it was seen that the process did deposit some molten material on the bottom side of the cutting kerf, a tendency not seen for the RFC samples.

4. Conclusion

In this paper, the quality of remote DOE cutting has been experimentally examined. Two methods were used for analyzing the quality. One was an automatic measurement system for mass evaluation of all 1200 cut samples. The other was a manual cutting, polishing and etching process that gave qualitative data for 20 selected samples.

From the automatic measurement system it was determined that the majority of cuts were obtained with kerf widths between 100 and 200 µm. The standard deviation generally lies within 15 µm in the stable cutting regions with regard to velocity, focus, work angle, and travel angle. By analyzing 20 etched samples, data about the melt zone, perpendicularity and kerf widths were found. From these samples it was determined that the width of the molten material on the side of the cutting kerf is approximately 83% deeper for RFC than for RDC when comparing similar samples (70% if all samples were considered). Furthermore, the perpendicularity of the RDC cuts was approximately 46 µm better than for similar RFC cuts. Furthermore, it was noticed that the RDC process produces some minor burr on the bottom side of the cutting kerf when compared to RFC. However, the 83% reduction in melt layer thickness was obtained with cutting speeds close to 20% of the cutting speeds of RFC. Furthermore, due to the 21% duty cycle of the process, the required average power was only 630W, which is lower than the power required for RFC (approx. 3kW).

Acknowledgements

This work was supported in part by the Danish National Advanced Technology Foundation and our industrial partners IPU, Grundfos, Volvo, Kuka, Ib Andresen and Micronix. Equipment used for this work was supported by the Poul Due Jensen Foundation.

References

Lu, Jinhong, and Veli Kujanpää. 2013. “Review study on remote laser welding with fiber lasers.” Journal of Laser Applications 25 (5)

Zaeh, M.F., J. Moesl, J. Musiol, and F. Oefele. 2010. “Material processing with remote technology revolution or evolution?” Physics Procedia 5, Part A (0): 19-33.

Matti, R. S., T. Ilar, and A. F. H. Kaplan. 2013. “Analysis of laser remote fusion cutting based on a mathematical model.” Journal of Applied Physics 114 (23)

Schäfer, Peter. 2010. “Cutting at a distance.” *ATZproduktion worldwide* (Springer Automotive Media) 3 (2): 8-11.

Pihlava, Anssi, Tuomas Purtonen, Antti Salminen, Veli Kujanpää, and Timo Savinainen. 2013. “Quality aspects in remote laser cutting.” Welding in the World (Springer-Verlag) 57 (2): 179-187.

Villumsen, S., and Kristiansen, M. (2015) Angular stability margins for the remote fusion cutting process. Physics Procedia 78, 89 – 98. 15th Nordic Laser Materials Processing Conference, Nolamp 15.

Villumsen L. S. & Kristiansen, M. Olsen, F. O. (2016) On the stability and performance of remote DOE laser cutting, Physics Procedia, Volume 83, 2016,

Olsen, Flemming O.(2011) Laser cutting from CO2-laser to disc- or fibre laser – possiblities and challenges. In ICALEO,.

Olsen, Flemming O.(2009) Klaus Schütt Hansen, and Jakob Skov Nielsen. 2009. “Multibeam fiber laser cutting.” Journal of Laser Applications (Laser Institute of America) 21 (3): 133-138.

ISO (2002). International Organization for Standardization. Thermal cutting — Classification of thermal cuts — Geometrical product specification and quality tolerances. ISO 9013:2002(E).